Chinese Chemical Letters 34 (2023) 107222

Contents lists available at ScienceDirect

Chinese Chemical Letters

journal homepage: www.elsevier.com/locate/cclet

# Mn-N-P doped carbon spheres as an efficient oxygen reduction catalyst for high performance Zn-Air batteries

Jiajie Li[a,1], Shanbao Zou[a,1], Jinzhen Huang[b], Xiaoqian Wu[a], Yue Lu[a], Xundao Liu[a], Bo Song[b,*], Dehua Dong[a,*]

[a] School of Materials Science and Engineering, University of Jinan, Ji'nan 250022, China
[b] National Key Laboratory of Science and Technology on Advanced Composites in Special Environments, Harbin Institute of Technology, Harbin 150001, China

ARTICLE INFO

*Article history:*
Received 17 December 2021
Revised 16 January 2022
Accepted 14 February 2022
Available online 18 February 2022

*Keywords:*
Oxygen reduction reaction
Zn-air batteries
Transition metal
Doped carbon spheres

ABSTRACT

Low-cost and efficient oxygen reduction reaction (ORR) electrocatalysts are the key to developing Zn-air batteries for renewable energy storage. Herein, the Mn-N-P doped carbon sphere was prepared through polymerization of hexachlorotripolyphosphazene (HCCP) and phloroglucinol, and then followed the calcination at 900 °C. Theory calculations demonstrated the introduction of Mn in N-P doped carbon could lower the dissociation barrier of $O_2$ into O* and promote the ORR through a $4e^-$ pathway. The as-prepared catalysts exhibited a half-wave potential of 0.82 V *vs.* RHE and limiting current density of 5.2 mA/cm$^2$ toward ORR, which was comparable to those of the commercial Pt/C catalysts. In addition, Zn-air batteries with 0.05 Mn-N-P-C catalysts showed a high specific capacity of 830 mAh/$g_{Zn}$ and excellent cycle stability. This facile approach demonstrated herein could be a solution to develop optimum non-precious metal catalysts for the application in cathodes of proton exchange membrane fuel cells. This study also provides new insight to design the catalysts of multi-heteroatom coordinated metal in the carbon matrix for both fundamental researches and practical applications.



Ever-increasing energy consumption and environmental pollution have stimulated the development of renewable energy technology [1–4]. Recently, Zn-air batteries have become promising owing to their high efficiencies in renewable energy storage [5–8]. However, the sluggish oxygen reduction reaction that occurs at the cathode side significantly limits their energy conversion efficiency [9–11]. Therefore, it is necessary to develop efficient electrocatalysts for ORR [12–14]. Although precious metals (Pt, Ru and Ir) have been demonstrated to show high catalytic activity, their high cost and low stability restrain their practical applications [15–17]. The investigation on low-cost and efficient ORR electrocatalysts is therefore important to develop high performance Zn-air batteries [18–20].

Many efforts have been devoted to developing highly-active ORR catalysts with different compositions and structures, such as carbon materials [21–24], perovskites [25–27], and transition metal nitrides/phosphides [28–30]. Among them, carbon materials have received extensive attention due to their low-cost, large specific surface area, and good electrical conductivity [31–33]. It has been demonstrated that N-doing could change the electrochemical properties of carbon materials and thereby enhance ORR catalytic activity, due to the formation of adjacency between carbon atoms and pyridine nitrogen [34–36]. However, the ORR catalytic activity of N-doped carbon is still lower than commercial Pt/C catalysts [37,38]. Introducing transition metals (Fe, Co, Mn *etc.*) to N-doped carbon could change the bonding of carbon matrix and expose more active sites, and thus further enhance the ORR activity [39–44]. Among all the transition-metal-doped carbon materials, Fe-N-C catalysts present high catalytic activity for ORR. However, the loss of Fe species into electrolytes under electrochemical oxidation conditions leads to the degradation in activity, thus improving the stability is still challenging [45]. Compared to Fe-N doped carbon materials, Mn-N doped carbon materials have been demonstrated to show better stability, [46] however, relatively inferior activity towards ORR, due to the electronic configuration and D-band structure of Mn atoms [47]. Theoretical results demonstrated that the strong interaction between Mn-N active sites and the ORR intermediate (*e.g.*, O*, OH*) would lead to a $2e^-$ ORR to produce $H_2O_2$ [48,49]. Recent studies have revealed that the ORR performance of such M-N-C catalysts could be further improved by introducing the third kind of heteroatoms [50,51]. For example,

* Corresponding authors.
*E-mail addresses:* songbo@hit.edu.cn (B. Song), mse_dongdh@ujn.edu.cn (D. Dong).
[1] These authors contributed equally to this work.

https://doi.org/10.1016/j.cclet.2022.02.027
1001-8417/

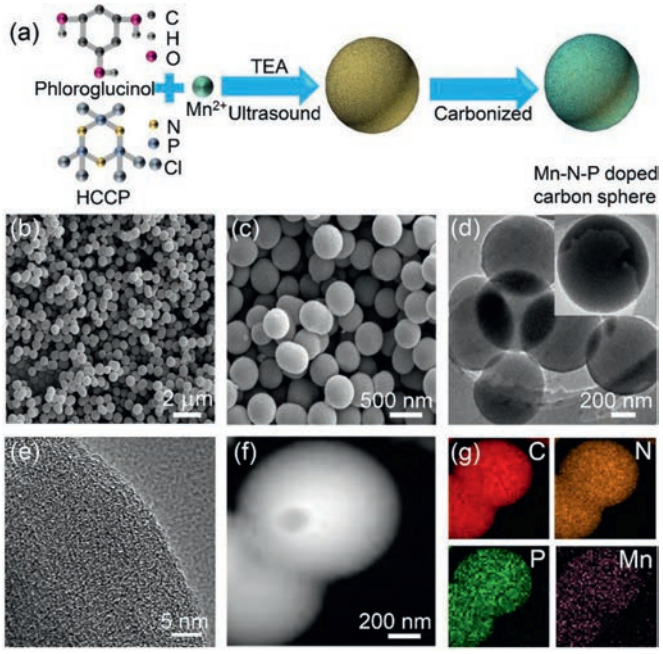


**Fig. 1.** (a) The schematic diagram for synthesizing Mn-N-P doped carbon spheres (*x*Mn-N-P-C) electrocatalysts, (b, c) FESEM images, (d-f) TEM images and (g) elemental mapping of C, N, P and Mn in 0.05 Mn-N-P-C spheres.

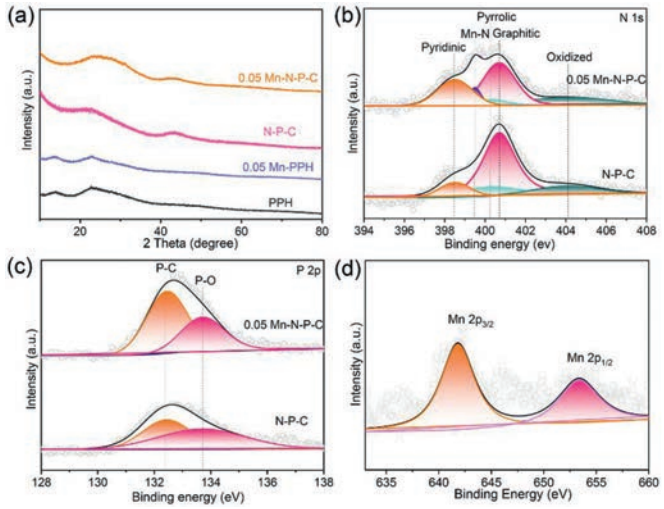


**Fig. 2.** Analyses on the structure and surface chemical valence state of 0.05 Mn-N-P-C. (a) XRD patterns of 0.05 Mn-PPH, PPH, 0.05 Mn-N-P-C and N-P-C. (b) N 1s and (c) P 2p XPS survey spectra of 0.05 Mn-N-P-C and N-P-C. (d) Mn 2p XPS spectra of the 0.05 Mn-N-P-C.

Hu *et al.* reported that the introduction of cobalt atoms into the N-P-C system improved the ORR catalytic performance by promoting the oxygen absorption with the interaction between cobalt atoms and P-N-C [50]. Li *et al.* introduced Fe into the N-P-C system to improve ORR catalytic performance and found out that dispersed Fe-N-P-C-O complex was the dominant active sites [51]. Zhu *et al.* found out that introducing phosphorus atoms into the Mn-N system to form N, P co-coordinated Mn sites ($MnN_xP_y$) also could promote the ORR process [47]. However, to achieve the rational design of high-performance Mn-N-P doped carbon catalysts and the understandings on inherent ORR kinetics, more efforts are still needed from both experimental and theoretical aspects.

Herein, Mn-N-P doped carbon spheres were synthesized through a two-step strategy involving the adsorption of Mn elements during polymerization process and then the carbonization with a pyrolysis process. The as-prepared catalysts exhibited high electrocatalytic activity and outstanding stability for ORR. Theory calculations demonstrated the Mn-N-P doped carbon showed lower energy toward $4e^-$ ORR. In addition, Zn-air batteries with 0.05 Mn-N-P-C catalysts as the cathode showed a high specific capacity of 830 mAh/$g_{Zn}$ and good cycle stability.

The Mn-N-P doped carbon spheres were synthesized by the polymerization of hexachlorotripolyphosphazene (HCCP) and phloroglucinol under the presence of $Mn^{2+}$, followed by a carbonization process, as shown in Fig. 1a. The morphology of the as-synthesized catalysts was characterized by scanning electron microscope (SEM) and transmission electron microscopy (TEM). As shown in Fig. 1b and Fig. S1 (Supporting information), the synthesized Mn-doped phosphosphazene microsphere (Mn-PPH) precursors exhibit a sphere morphology with an average diameter of ~700 nm, which is similar to that of the PPH without Mn, suggesting the addition of $Mn^{2+}$ in the polymerization will not significantly affect the morphology. After carbonization, the sphere morphology was well preserved (Fig. 1c and Fig. S1 in Supporting information) while the diameter was reduced to ~500 nm. Noteworthily, the 0.05 Mn-N-P-C catalyst exhibited a smooth surface (Fig. 1d and inset) without metal-related particles on it and the respective selected area electron diffraction (SAED, Fig. S2 in Supporting information) pattern implies its amorphous state. High-resolution TEM image (Fig. 1e) also demonstrated that amorphous carbon structures were dominant in the sphere. Furthermore, elemental mappings of 0.05 Mn-N-P-C catalyst in Figs. 1f and g showed that the Mn, N and P are distributed uniformly throughout the carbon spheres, suggesting that Mn, N and P were doped into the carbon matrix successfully.

The structural properties of the as-prepared spheres were revealed by X-ray diffractometer (XRD). As shown in Fig. 2a and Fig. S3 (Supporting information), 0.05 Mn-PPH showed a similar XRD pattern as the PPH. After carbonization process, both the 0.05 Mn-N-P-C and N-P-C catalysts exhibited one broad peak at around 24.6°, which could be indexed to graphitic carbon. In XRD patterns of Mn-N-P doped sphere, Mn-related characteristic diffraction peaks were not observed, which was consistent with the TEM results. Raman spectra of the N-P-C and Mn-N-P-C catalysts (Fig. S4 in Supporting information) has two characteristic peaks corresponding to the D (1327.7 $cm^{-1}$) and G (1587.6 $cm^{-1}$) bans of graphite carbon which consisted with the XRD results [52]. Furthermore, the $I_D/I_G$ ratios of Mn-N-P doped samples lower than that of N-P-C, suggesting that the Mn doped samples have higher graphitization degree and favors the electron transfer [53]. The surface chemical structure of the as-prepared Mn-N-P-C catalysts was investigated by X-ray photoelectron spectroscopy (XPS). As shown in Table S1 (Supporting information), Mn-N-P-C catalysts showed the presence of Mn, N and P elements, well matching with the elemental mapping analysis. Inductively coupled plasma mass spectrometry (ICP-MS, Table S2 in Supporting information) confirms the Mn and P content in the as synthesized samples. The loading amount of Mn was about 1.02 wt%, 1.54 wt% and 2.43 wt% for 0.025 Mn-N-P-C, 0.05 Mn-N-P-C and 0.1 Mn-N-P-C, respectively. The contents of Mn element were increased along with the increase of Mn precursors, indicating the Mn content could be well controlled.

High resolution N 1s XPS spectra could be deconvoluted into four main peaks, namely pyridinic N (398.3 eV), pyrrolic N (400.1 eV), graphitic N (400.7 eV) and oxidized N (404.1 eV) (Fig. 2b and Fig. S5 in Supporting information) [45,54]. These peaks confirmed the successful integration of N into the carbon matrix. Notably, for Mn doped catalysts, an obvious Mn-N peak at 399.5 eV was detected [45,55]. It has been reported that the formation of

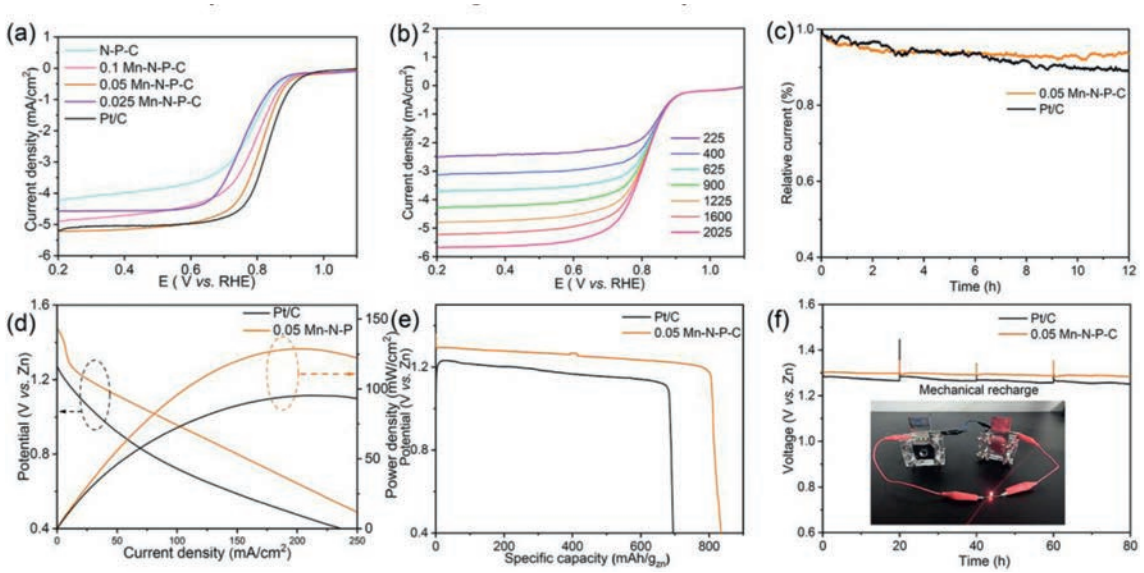


**Fig. 3.** ORR and primary Zn-air battery performance of 0.05 Mn-N-P-C catalyst. (a) LSV curves for Pt/C, Mn-N-P-C and N-P-C catalysts, (b) LSV curves of 0.05 Mn-N-P-C at various rotating speeds, (c) long-term durability test of the 0.05 Mn-N-P-C and commercial Pt/C catalysts in the 0.1 mol/L $O_2$-saturated KOH solution under the potential of 0.5 V *vs.* RHE, (d) discharging polarization curves and power density plots of primary Zn-air batteries, (e) specific capacity plots of the primary Zn-air batteries at 5 mA/cm$^2$, (f) long-term durability tests of the Zn-air battery at the current density of 10 mA/cm$^2$.

an Mn−N bond could improve the ORR catalytic activity [56,57]. P 2p spectra of the catalysts (Fig. 2c and Fig. S6 in Supporting information) showed two different peaks at 132.4 eV (P−C) and 133.7 eV (P−O), suggesting that the P were introduced into the carbon matrix [58–60]. In Mn doped catalysts, the Mn 2p XPS spectrum (Fig. 2d and Fig. S7 in Supporting information) displayed two peaks at 641.8 and 653.4 eV, which should be attributed to Mn $2p_{3/2}$ and Mn $2p_{1/2}$, respectively [45]. These results revealed that Mn, N, and P elements were successfully doped into the carbon matrix. Specifically, the Mn were bound to the N in the catalyst, which was demonstrated by the formation of Mn−N bond in the as-synthesized carbon sphere.

ORR performance of the catalysts was investigated in $N_2$ or $O_2$ saturated 0.1 mol/L KOH. As shown in Fig. S8 (Supporting information), no peak was detected in the CV curves of Mn-N-P-C under $N_2$ saturation solution. On the contrary, an obvious reduction peak at 0.78 V *vs.* RHE was observed for 0.05 Mn-N-P-C catalyst in $O_2$-saturated solutions, suggesting ORR process was conducted over the catalysts in the presence of $O_2$. Additionally, the reduction peak of 0.05 Mn-N-P-C catalyst present a positive shift of 60 mV compared to the N-P doped carbon catalyst (Fig. S8 in Supporting information), which indicated the introduction of Mn can enhance the ORR performance. Fig. 3a showed the LSV curves of the N-P, Mn-N-P-C and commercial Pt/C catalysts at the rotation rate of 1600 rpm. As expected, compared to the N-P doped sample, the limiting current density and half-wave potential were improved obviously after the introduction of Mn. The 0.05 Mn-N-P-C catalyst showed a limiting current density of 5.2 mA/cm$^2$ with a half-wave potential of 0.82 V *vs.* RHE, which was the highest ORR catalytic activity compared to other Mn-N-P and N-P doped carbon catalysts. Moreover, 0.05 Mn-N-P-C catalyst showed comparable ORR performance with commercial Pt/C catalysts and a higher ORR performance to some recently-reported Metal-N-P doped carbon catalysts (Table S3 in Supporting information). According to the above results, the N, P co-doped samples have poor ORR activity [50]. In comparation, after introduction Mn element in those samples, the ORR performance has a significant improvement. It can be concluded that the introduction of Mn could increase the intrinsic active sites of the catalysts, which led to a lower over-potential and a higher current density during the ORR. To further reveal the ORR kinetics of all catalysts, LSV curves (Fig. 3b and Fig. S9 in Supporting information) were collected at different rotation speeds. The limiting current density of 0.05 Mn-N-P-C catalyst increased steadily with the rotational speed. Koutecky-Levich (K-L) equation was used to determine the electron transfer number per oxygen molecule ($n$) for the ORR (Fig. S10 in Supporting information). The $n$ for 0.05 Mn-N-P-C was ~3.9, indicating that the ORR was majorly conducted through a 4e$^-$ ORR pathway. As shown in Fig. S11 (Supporting information), the corresponding kinetic parameters were analyzed with the K-L equation and the 0.05 Mn-N-P-C catalyst exhibited the highest $J_k$ (17.4 mA/cm$^2$ at 0.4 V *vs.* RHE) among other N-P and Mn-P-N doped catalysts. Moreover, during the long-term *i-t*-test, the current density of 0.05 Mn-N-P-C was maintained at about 93.8% (*versus* 88% for commercial Pt/C catalysts, Fig. 3c) and the LSV curves has a slightly decrease (Fig. S12 in Supporting information) which indicated that the as-synthesized Mn-N-P doped carbon sphere had better stability towards ORR compared to commercial Pt/C. The structure of 0.05 Mn-N-P-C catalysts after stability test was characterized as shown in Fig. S13 (Supporting information) which maintains a stable spherical structure. More importantly, after long-term test, the Mn, N and P are still distributed uniformly throughout the carbon spheres (Fig. S14 in Supporting information) demonstrated that the 0.05 Mn-N-P-C catalyst was stable during ORR process. All the above results indicated that the as-synthesized 0.05 Mn-N-P-C catalyst has high ORR activity and good stability.

The high ORR performance of 0.05 Mn-N-P-C catalyst was further tested in primary Zn-air batteries. The Zn-air battery was assembled by using 0.05 Mn-N-P-C catalyst (commercial Pt/C catalyst was also used for comparison) as air cathode catalyst and a Zn sheet as an anode in a special battery case filled with 6 mol/L KOH electrolyte. As shown in Fig. 3d, Zn-air batteries with 0.05 Mn-N-P-C catalyst exhibited a higher open circuit voltage (OCV) of 1.45 V and maximum power density of 133 mW/cm$^2$ compared to those of commercial Pt/C catalysts (1.28 V and 98 mW/cm$^2$), which were also higher than those recently reported in literature (Table S4 in Supporting information). To further study the capacity performance of the Zn-air batteries, discharge tests were performed (Fig. 3e). When normalized to the consumption mass of Zn, the battery with 0.05 Mn-N-P-C catalyst had a specific capacity of about 830

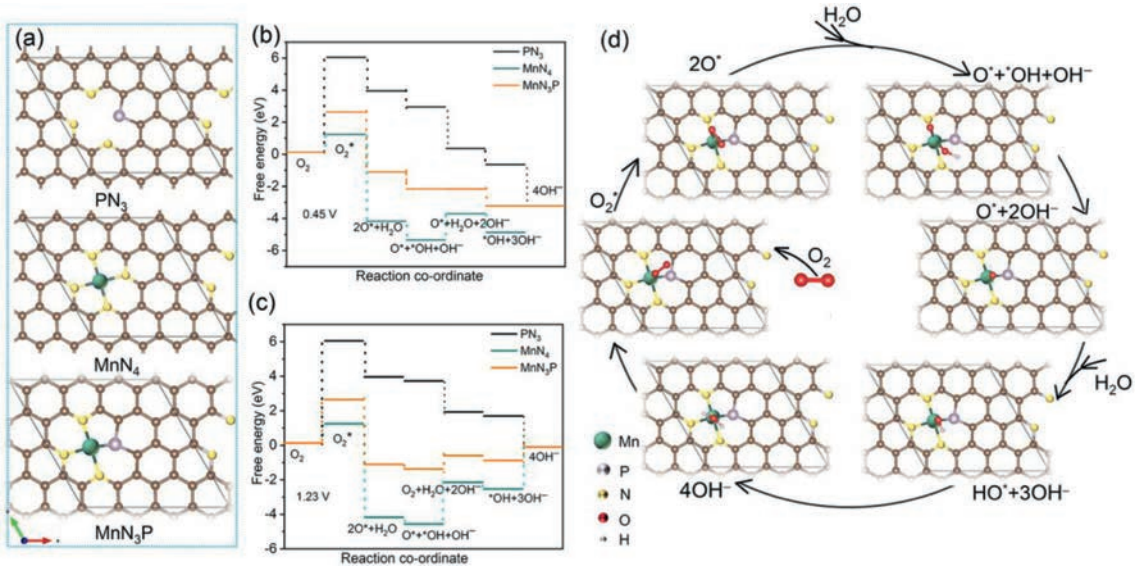


**Fig. 4.** DFT calculation. (a) The schematic atomic structures of $PN_3$, $MnN_4$ and $MnN_3P$ used for the DFT calculations and the calculated free energy evolution diagrams of ORR at (b) $U = 1.23$ V and (c) $U = 0.45$ V, (d) the schematic illustration for the ORR pathway as predicted from the calculation.

$mAh/g_{Zn}$, which was superior to that of the commercial Pt/C catalysts (700 $mAh/g_{Zn}$). Furthermore, discharges at different current densities showed no significant potential drop, suggesting good stability of the 0.05 Mn-N-P-C cathode catalyst (Fig. S15 in Supporting information). Fig. 3f indicated that the battery could be mechanically recharged multiple times without obvious degradation on potential. Finally, two Zn-air batteries were connected in series to produce an OCV of ~2.5 V, which was able to power the light emitting diodes (Fig. 3f, inset).

From the above results, Mn-N-P doped catalyst showed higher ORR activity compared to that of N-P doped sample. XPS results indicated that the formation of Mn−N and P−C bonds in the catalyst. To elucidate the active sites and reaction mechanism for ORR, density functional theory (DFT) calculations were carried out. The optimized atomic structures for $PN_3$, $MnN_4$ and $MnN_3P$ were schematically illustrated in Fig. 4a. The free-energy profiles of ORR process were then calculated at $U = 0.45$ and 1.23 V respectively. As shown in Figs. 4b and c, oxygen adsorption step of $PN_3$, $MnN_4$ and $MnN_3P$ required high activation energies both at 1.23 V and 0.45 V. In all the atomic structures, $PN_3$ has the highest oxygen adsorption energy (about 6.05 eV) thus the ORR is difficult to occur. For $MnN_4$, it has the lowest adsorption energy of about 1.25 eV for the reaction of $O_2$ into $O_2^*$. However, the free energy of hydrogenation of adsorbed *OH to $OH^-$ needs an activation barrier of 2.43 eV and 1.65 eV at 1.23 V and 0.45 V, respectively (Figs. 4b-d). In all the optimized atomic structures, $MnN_3P$ has the intermediate adsorption energy of about 2.65 eV. Compared to the $MnN_4$ structure, $MnN_3P$ has lower activation barriers of 0.78 eV and 0 eV at 1.23 V and 0.45 V respectively (Figs. 4b-d), which suggest the $MnN_3P$ has appropriate reaction energy to promote the ORR along the $4e^-$ associative pathway. The experimental and calculated results indicated that the introduction of Mn element in N-P doped carbon can lower the dissociation barrier of $O_2$ into $O^*$ and promote the ORR to follow a $4e^-$ associative pathway.

In conclusion, Mn-N-P doped carbon spheres were prepared through the polymerization followed by calcination at 900 °C. The as-prepared Mn-N-P doped carbon catalysts exhibited high electrocatalytic activity and good stability for ORR. Zn-air batteries with 0.05 Mn-N-P-C catalysts showed a higher specific capacity and good cycle stability compared to those of Pt/C. Theoretical calculations demonstrated the introduction of Mn in N-P doped carbon can lower the dissociation barrier of $O_2$ into $O^*$ and benefit the reaction coordinate to follow the $4e^-$ ORR pathway. Therefore, the Mn-N-P-C catalyst developed in this study can be the promising alternative to commercial Pt/C catalysts in Zn-air batteries.

## Declaration of competing interest

The authors report no declarations of competing interests.

## Acknowledgments

This work was financially supported by the Science and Technology Program of University of Jinan (Nos. XKY2103, XKY2105), National Natural Science Foundation of China (Nos. 51902130, 52072085) and Key Research and Development project of Shandong Province (No. 2019GGX102087).

## Supplementary materials

Supplementary material associated with this article can be found, in the online version, at doi:10.1016/j.cclet.2022.02.027.

## References

[1] J. Huang, H. Sheng, R.D. Ross, et al., Nat. Commun. 12 (2021) 3036.
[2] R. Wang, J. Han, P. Xu, et al., Adv. Sci. 7 (2020) 2000216.
[3] X. Wang, Y. Wang, X. Sang, et al., Angew. Chem. Int. Ed. 60 (2021) 4192–4198.
[4] T.J. Wang, F.M. Li, H. Huang, et al., Adv. Funct. Mater. 30 (2020) 2000534.
[5] L. Liu, G. Zeng, J. Chen, et al., Nano Energy 49 (2018) 393–402.
[6] S. Hu, T. Han, C. Lin, et al., Adv. Funct. Mater. 27 (2017) 1700041.
[7] X. Han, X. Wu, C. Zhong, et al., Nano Energy 31 (2017) 541–550.
[8] Q. Fu, X. Wang, J. Han, et al., Angew. Chem. Int. Ed. 60 (2021) 259–267.
[9] Y. Nie, L. Li, Z. Wei, Chem. Soc. Rev. 44 (2015) 2168–2201.
[10] K. Iwase, T. Yoshioka, S. Nakanishi, et al., Angew. Chem. Int. Ed. 54 (2015) 11068–11072.
[11] T.Y. Jeon, S.H. Yu, S.J. Yoo, et al., Carbon Energy 3 (2021) 375–383.
[12] S. Chang, H. Zhang, Z. Zhang, J. Energy Chem. 56 (2021) 64–71.
[13] S. Li, Z.Q. Tian, Y. Liu, et al., Chin. J. Catal. 42 (2021) 648–657.
[14] C. Su, Y. Liu, Z. Luo, et al., Chem. Eng. J. 406 (2021) 126883.
[15] G. Wan, P. Yu, H. Chen, et al., Small 14 (2018) 1704319.
[16] H. Zhang, H.T. Chung, D.A. Cullen, et al., Energy Environ. Sci. 12 (2019) 2548–2558.
[17] T.J. Wang, H.Y. Sun, Q. Xue, et al., Sci. Bull 66 (2021) 2079–2089.
[18] S. Zhang, O. Oms, L. Hao, et al., ACS Appl. Mater. Interfaces 9 (2017) 38486–38498.
[19] M.J. Wang, Z.X. Mao, L. Liu, et al., Small 14 (2018) 1804183.
[20] T. Najam, S.S.A. Shah, W. Ding, et al., Angew. Chem. Int. Ed. 57 (2018) 15101–15106.
[21] Q. Qin, H. Jang, P. Li, et al., Adv. Energy Mater. 9 (2019) 1803312.

[22] Y. Liu, B. Huang, X. Zhang, et al., J. Power Sources 412 (2019) 125–133.
[23] Y. Wang, E. Luo, X. Wang, et al., Chin. Chem. Lett. 32 (2021) 506–510.
[24] X. Qin, D. Kim, Y. Piao, Carbon Energy 3 (2021) 66–100.
[25] Y. Sun, Z. Liu, W. Zhang, et al., Small 15 (2018) 1803513.
[26] M. Retuerto, F. Calle-Vallejo, L. Pascual, et al., ACS Appl. Mater. Interfaces 11 (2019) 21454–21464.
[27] H. Lee, O. Gwon, C. Lim, et al., ChemElectroChem 6 (2019) 3154–3159.
[28] Y. Yuan, J. Wang, S. Adimi, et al., Nat. Mater. 19 (2019) 282–286.
[29] Q. Fu, J. Han, X. Wang, et al., Adv. Mater. 33 (2021) 1907818.
[30] X. Wang, X. Sang, C.L. Dong, et al., Angew. Chem. Int. Ed. 60 (2021) 11959–11965.
[31] X. Hu, Y. Chen, M. Zhang, et al., Carbon 144 (2019) 557–566.
[32] J. Ding, P. Wang, S. Ji, et al., Electrochim. Acta 296 (2019) 653–661.
[33] B. Liu, H. Zhou, H. Jin, et al., Chin. Chem. Lett. 32 (2021) 535–538.
[34] X.R. Wang, J.Y. Liu, Z.W. Liu, et al., Adv. Mater. 30 (2018) 1800005.
[35] J. Li, Y. Zhang, X. Zhang, et al., ACS Appl. Mater. Interfaces 9 (2017) 398–405.
[36] J. Huang, J. Han, T. Gao, et al., Carbon 124 (2017) 34–41.
[37] M. Borghei, N. Laocharoen, E. Kibena-Põldsepp, et al., Appl. Catal. B 204 (2017) 394–402.
[38] J. Zhang, L. Dai, Angew. Chem. Int. Ed. 55 (2016) 13296–13300.
[39] J. Zhu, M. Xiao, G. Li, et al., Adv. Energy Mater. 10 (2019) 1903003.
[40] L. Liu, Y. Wang, F. Yan, et al., Small Methods 4 (2019) 1900571.
[41] M. Qiao, Y. Wang, Q. Wang, et al., Angew. Chem. Int. Ed. 59 (2020) 2688–2694.
[42] H. Zhao, Y. Zhang, L. Li, et al., Chin. Chem. Lett. 32 (2021) 140–145.
[43] S. Zou, J. Li, X. Wu, et al., Chem. Phys. Lett. 778 (2021) 138769.
[44] X. Wang, S. Feng, W. Lu, et al., Adv. Funct. Mater. 31 (2021) 2104243.
[45] J. Li, M. Chen, D.A. Cullen, et al., Nat. Catal. 1 (2018) 935–945.
[46] G. Yang, J. Zhu, P. Yuan, et al., Nat. Commun. 12 (2021) 1734.
[47] X. Zhu, R. Amal, X. Lu, Small 15 (2019) 1804524.
[48] K. Liu, Z. Qiao, S. Hwang, et al., Appl. Catal. B 243 (2019) 195–203.
[49] H. Cao, G.J. Xia, J.W. Chen, et al., J. Phys. Chem. C 124 (2020) 7287–7294.
[50] X.L. Hu, X.H. Dai, X.Q. He, New J. Chem. 41 (2017) 15236–15243.
[51] Y. Li, B. Chen, X. Duan, et al., Appl. Catal. B 249 (2019) 306–315.
[52] L. Wei, L. Qiu, Y. Liu, et al., ACS Sustain. Chem. Eng. 7 (2019) 14180–14188.
[53] X. Feng, Y. Bai, M. Liu, et al., Energy Environ. Sci. 14 (2021) 2036–2089.
[54] Y. Yang, K. Mao, S. Gao, et al., Adv. Mater. 30 (2018) 1801732.
[55] Y.Z. Chen, C. Wang, Z.Y. Wu, et al., Adv. Mater. 27 (2015) 5010–5016.
[56] M. Yu, L. Wang, J. Liu, et al., ACS Appl. Mater. Interfaces 11 (2019) 17482–17490.
[57] S. Gong, C. Wang, P. Jiang, et al., J. Mater. Chem. A 6 (2018) 13254–13262.
[58] J. Zhang, Z. Zhao, Z. Xia, L. Dai, Nat. Nanotechnol. 10 (2015) 444–452.
[59] Q. Fu, X. Wang, J. Han, et al., Angew. Chem. Int. Ed. 60 (2021) 259–267.
[60] J. Huang, P. Xu, T. Gao, et al., ACS Sustain. Chem. Eng. 8 (2020) 1319–1328.